Dynamic Correction of Artifacts due to Susceptibility Effects and Time-Varying Eddy Currents in DTI

T-K. Truong[1], N-K. Chen[1], and A. W. Song[1]
[1]Brain Imaging and Analysis Center, Duke University, Durham, NC, United States

Introduction

Diffusion tensor imaging (DTI) is a powerful technique for assessing white matter connectivity and integrity noninvasively. However, it is vulnerable to spatial and temporal variations of the static magnetic field (B_0) caused by susceptibility effects near air/tissue interfaces, $B_0^{SUSC}(\mathbf{x})$, and eddy currents induced by the diffusion gradients, $B_0^{EDDY}(\mathbf{x}, t, d)$. The dependence on space ($\mathbf{x}$), time (t), and diffusion direction (d) causes distortions, blurring, and misregistration among diffusion-weighted images, which in turn lead to errors in the derivation of the diffusion tensor and hence in fractional anisotropy (FA) maps and in fiber tractography.

Existing correction methods such as B_0 mapping (1,2), reversed gradient polarity (3–5), and post-processing (6,7) assume that B_0^{EDDY} remains constant within the readout window T_{ACQ}, whereas the widely used twice refocused spin-echo (TRSE) method (8) assumes that it decays monoexponentially, which is known not to be the case. Here, we propose a novel dynamic correction method that measures the exact time dependence of B_0^{EDDY} within T_{ACQ} and accurately corrects for both B_0^{SUSC}- and B_0^{EDDY}-induced artifacts.

Methods

Dynamic B_0^{EDDY} mapping is performed by acquiring a train of asymmetric spin-echo images at increasing TEs (t_1, …, t_N) spanning T_{ACQ} (Fig. 1). The phase images are unwrapped along the TE dimension and, for each t_n, fitted with $\phi(t) = \phi_0(t_n) + \gamma\, B_0^{EDDY}(t_n)\, t$, where ϕ_0 is a constant, γ is the gyromagnetic ratio, and t is a 3-point moving window $\{t_{n-2}, t_n, t_{n+2}\}$. This procedure is performed separately on odd and even echoes to avoid errors due to off-resonance effects. Since B_0^{EDDY} varies slowly in space, the B_0^{EDDY} maps are fitted with a 3rd order polynomial function in space to improve the signal-to-noise ratio. Static B_0^{SUSC} mapping is performed with the same pulse sequence by fitting all echoes instead of using a moving window.

Since B_0^{EDDY} is subject-independent but diffusion direction-dependent, the B_0^{EDDY} mapping only needs to be performed once on a spherical gel phantom, but with the same diffusion-weighting scheme as the DTI scan. Conversely, since B_0^{SUSC} is subject-dependent but diffusion-independent, the B_0^{SUSC} mapping is performed *in vivo*, but without diffusion-weighting.

Dynamic correction of B_0^{SUSC}- and B_0^{EDDY}-induced artifacts is then performed as follows (Fig. 2). For each $t_n = t_1, \ldots, t_N$ corresponding to the acquisition a k_y line in k-space, the uncorrected DTI image is multiplied by $\exp[-i\phi(\mathbf{x}, t_n, d)]$, where $\phi(\mathbf{x}, t_n, d) = \gamma \int_0^{t_n} [B_0^{SUSC}(\mathbf{x}) + B_0^{EDDY}(\mathbf{x}, t, d)]dt$. Each of these N images is Fourier transformed to k-space, and the n^{th} k_y line (acquired at time t_n) is extracted from the n^{th} k-space to form a new k-space, which is then inverse Fourier transformed to yield the corrected image.

We studied a healthy volunteer on a 3 T GE scanner using TR = 5 s, TE = 73 ms, matrix size = 96×96, voxel size = (2.5 mm)^3, 5/8 partial Fourier, b = 1000 s/mm^2, 15 diffusion directions, and T_{ACQ} = 57 ms. For comparison with the proposed dynamic correction, a static correction was also performed using the B_0^{SUSC} map as well as static $B_0^{EDDY}(\mathbf{x}, d)$ maps computed by fitting all echoes instead of using a moving window.

Results and Discussion

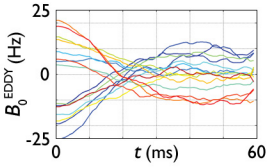

Fig. 3: B_0^{EDDY} time courses within T_{ACQ} in a given voxel for 15 diffusion directions.

Fig. 3 shows that B_0^{EDDY} varies significantly within T_{ACQ} for all diffusion directions. Furthermore, the zero-crossing clearly shows that it cannot be modeled as a single exponential decay, as assumed in the TRSE method, due to the presence of multiple eddy currents with different time constants. Repeated measurements over 6 weeks yielded identical results, showing that the phantom B_0^{EDDY} mapping can be performed infrequently, which makes the proposed method very efficient.

The uncorrected FA maps show severe B_0^{SUSC}-induced distortions around the ventricles and the genu of the corpus callosum (Fig. 4A, dashed lines) as well as B_0^{EDDY}-induced FA errors at the anterior (yellow arrows) and posterior (red arrows) edges of the brain. The static correction can only correct for the B_0^{SUSC}-induced distortions and the B_0^{EDDY}-induced FA errors at the posterior edge of the brain, but not at the anterior edge (Fig. 4B, yellow arrows). On the other hand, the dynamic correction can effectively correct for all artifacts (Fig. 4C).

Although B_0^{SUSC}- and B_0^{EDDY}-induced artifacts may appear fairly localized, a subtraction between the uncorrected and corrected FA maps reveals that they are actually significant throughout the whole brain (Fig. 5A). Similarly, a comparison between the static and dynamic correction shows that residual B_0^{EDDY}-induced artifacts are still widespread and can result in up to 30% errors in FA values (Fig. 5B).

These results demonstrate that it is important to take into account the exact time dependence of B_0^{EDDY} within T_{ACQ} and that the proposed dynamic correction method can effectively and efficiently correct for both B_0^{SUSC}- and B_0^{EDDY}-induced artifacts, without requiring any additional scan time as compared to existing static B_0 mapping methods (1,2) and while providing a higher signal-to-noise ratio than the TRSE method.

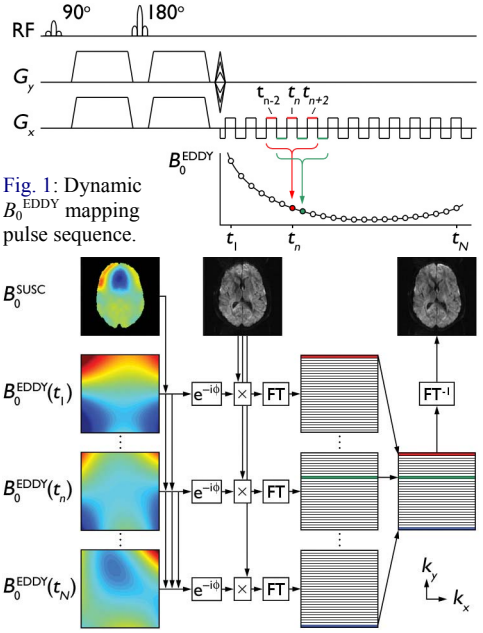

Fig. 1: Dynamic B_0^{EDDY} mapping pulse sequence.

Fig. 2: Dynamic artifact correction.

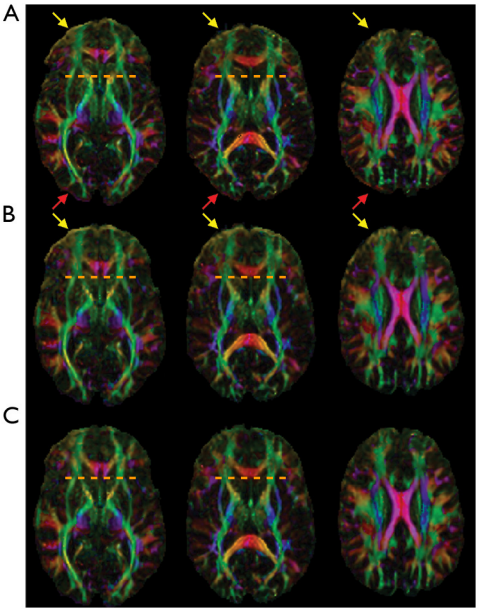

Fig. 4: Color-coded FA maps with no correction (A), static correction (B), and dynamic correction (C).

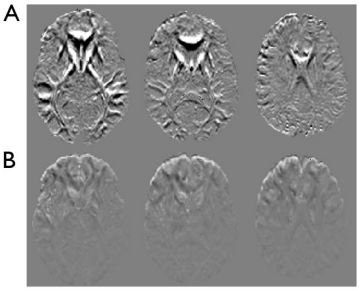

Fig. 5: FA difference maps for no vs. dynamic correction (A) and static vs. dynamic correction (B). Scale: ±0.3.

References

(1) Chen NeuroImage 2006;30:121 (2) Truong NeuroImage 2008;40:53 (3) Bodammer MRM 2004;51:188 (4) Shen MRM 2004;52:1184 (5) Andersson NeuroImage 2003;20:870 (6) Rohde MRM 2004;51:103 (7) Ardekani MRM 2005;54:1163 (8) Reese MRM 2003;49:177. Support: NIH grants NS41328 and NS65344.